JOURNAL OF MATERIALS SCIENCE 33 (1998) 3529–3539

Micromechanics of rubber–toughened polymers

XIAO-HONG CHEN, YIU-WING MAI
Centre for Advanced Materials Technology (CAMT), Department of Mechanical & Mechatronic Engineering J07, The University of Sydney, Sydney, NSW 2006, Australia
E-mail: mai@mech.eng.usyd.edu.au.

A new micromechanical model is provided to account for the full interaction between rubber particles in toughened polymers. Three-dimensional large deformation elastic–plastic finite element analysis is carried out to obtain the local stress and strain fields and then a homogenization method is adopted to obtain the effective stress–strain relation. The dependence of the local stress and strain distributions and effective stress–strain relation on phase morphology and mechanical properties of rubber particles is examined under various transverse constraints. The profile for the effective yield surface is obtained at four different particle volume fractions. It is shown that stress triaxiality affects significantly the effective yield stress and the local stress concentrations. Rubber cavitation and matrix shear yielding are two coupled toughening mechanisms; which one occurs first depends on the properties of rubber particles and matrix and the imposed triaxiality. Rubber cavitation plays an important role in the toughening process under high tensile triaxial stresses. Axisymmetric modelling may underestimate, and two-dimensional plane-strain modelling may overestimate, the inter-particle interaction compared with three-dimensional modelling.

1. Introduction

Studies of the inter-relationship between microstructure and macroscopic property have become increasingly important in order to gain a better scientific understanding of the mechanical behaviour of polymer blends and to develop new material microstructures. The evaluation of an effective stress–strain relation of a heterogeneous material from those of its constituents is a classic micromechanics problem. Aboudi [1] has given a comprehensive overview on this topic. Because the mathematics involved in determining the analytical solutions of the local stress and strain fields is often intractable for multiple-particle systems, numerical analysis is generally used. Tong and Mei [2] used two-scale and multi-scale methods for heterogeneous media to derive the effective constitutive relations for composite materials consisting of fibres and matrix. The periodic solutions at the micro- and meso-scale levels are first solved by the finite element method. These solutions are then used to establish the effective constitutive relations at the macro-scale level.

In recent years, the understanding of micromechanics and micromechanisms of rubber-toughened polymers has been greatly advanced through extensive experimental and theoretical work [3–5]. Two important toughening mechanisms are identified for rubber-modified epoxy and nylon, that is, localized shear yielding due to stress concentration at the equator of rubber particles and dilatation deformation due to the growth of voids formed by rubber cavitation or interfacial debonding [6–11]. Yee and co-workers [7–10] and Wu and Mai [11] reported experimental evidence on the pre-requisite of rubber cavitation to relieve the triaxial stress plane-strain condition associated with the crack tip for extensive plastic deformation to be developed in the matrix. On the other hand, Guild and Young [12] and Huang and Kinloch [13, 14] used cylindrical or two-dimensional plane-strain periodic cell models to study the toughening mechanisms in rubber-modified epoxy. They found that the rubber particles behave just like holes (because these authors used rather low bulk moduli of 66.67 and 33.33 MPa for the rubber particles). It seemed, therefore, that rubber cavitation and matrix shear yielding could be two independent toughening mechanisms. In a subsequent paper [15], Huang and Kinloch did recognize the problem of using a low Poisson's ratio of 0.49 for the rubber particles and they also discussed the influence of the rubber bulk modulus on the sequence of the toughening mechanisms. They clarified that rubber cavitation favours both extensive shear yielding and plastic hole growth in the epoxy matrix. Later, Bucknall *et al.* [16] also pointed out that the typical rubber bulk modulus should be around 2000 MPa and not as low as those used elsewhere [12–14]. Wu *et al.* [17, 18] studied the effects of volume fraction and bulk modulus of rubber particles on the constitutive relation and fracture toughness of rubber-modified polymers using two-dimensional plane-strain elastic–plastic finite element analysis. They confirmed that the rubber bulk modulus does have a significant effect on the hydrostatic tension in the rubber particles and on the plastic

deformation in the ligament between the crack tip and the particle. Guild and Kinloch [19, 20] have recently provided a spherical periodic cell model to investigate the stress distribution in rubber-modified epoxy under triaxial stress using axisymmetric elastic and elastic–plastic finite element analyses with proper consideration of the rubber bulk modulus in order to overcome the shortcomings of their previous model [13]. It is noted [12–14] that the cylindrical model is inherently inaccurate in that it reflects neither a regular distribution nor a random distribution of rubber particles and cannot predict coherent growth of a localized shear zone. The two-dimensional plane-strain model can successfully simulate the initiation and growth of the localized shear zone but cannot accurately describe the effect of rubber cavitation. The spherical model is based on the assumption that the overall effect of inter-particle interaction for random distribution is an "average" from all the neighbouring particles and not directional, which is reasonable for low volume fractions. The removal of all directional interactions in the spherical model may lead to an underestimation of the inter-particle interaction effect. The method of load application for the spherical model usually requires an iterative procedure, which is more complex than that for the cylindrical model or two-dimensional plane-strain model.

Owing to the complexity of and time required for three-dimensional problems, there have been very few studies on three-dimensional micromechanical modelling. Hom and McMeeking [21] pointed out that the coupling effects may be stronger in two-dimensional problems for cylindrical holes than in three-dimensional problems for initially spherical voids in their work on the void growth in an elastic–plastic material; but they were not concerned with rubber toughening mechanisms. Sue and Yee [22] gave a quite simple micromechanical model of the spherical rubber particle cavitation process at the crack tip using a combination of Irwin's crack-tip elastic analysis, slip-line field theory and Dewey's closed-form elastic solution. They incorporated the stress–strain fields around an existing plastic zone in front of the crack as the boundary condition to study the stress–strain field around a spherical rubber particle ahead of the crack tip. Chen and Tong [23] presented aligned and staggered periodic cell models to obtain the dependence of the effective elastic moduli of *in situ* liquid crystalline polymer LCP composites on spacing and aspect ratios, and arrangement of the orthotropic LCP phase. Chen and Mai [24] recently provided a three-dimensional periodic face-centred cuboidal cell model to study the effects of triaxiality on the toughening mechanisms of rubber-modified epoxy using three-dimensional elastoplastic finite element analysis. They found that rubber cavitation plays an important role in the toughening process under a high tensile triaxial stress state.

Sue and Yee [8] observed experimentally that shear yielding is initiated at the equator of particles, then shifts towards the pole around the interface and finally is localized to form shear bands in the direction of $\pm 45^\circ$ with the applied tensile stress. Huang and Kinloch [13, 14] used a two-dimensional plane-strain cell model with one particle surrounded by four neighbouring particles in a staggered layout to demonstrate successfully the observed localized shear zones. Hence, it seems that localized shear bands are formed more easily in a staggered periodic layout than in a regular periodic layout.

In this paper, we carry out three-dimensional large deformation elastic–plastic finite element analysis to study the effects of phase morphology and mechanical properties of particles on local stress concentration and the effective stress–strain relation under various constraint and loading conditions by a three-dimensional periodic cell model. In order to simulate both the cavitation and shear-banding processes, a face-centred cubic layout is chosen to represent the distribution of rubber particles in the matrix. Full three-dimensional interaction between particles is accounted for by prescribing periodic symmetry boundary conditions. The f c c layout is preferred to the b c c layout because it is easier to simulate the initiation and growth of shear bands. However, we have not performed the calculations to see if any significant difference would exist if b c c is used instead of f c c.

2. Micromechanical model

The matrix is assumed to be perfectly elastic–plastic governed by the Von Mises criterion and the rubber particles are elastic. The material properties used in the numerical study are given in Table I unless otherwise stated. The matrix has a Young's modulus of 3500 MPa, Poisson's ratio of 0.35 and yield strength of 80 MPa, which are typical of many commercially available epoxy resins.

A representative unit of the f c c periodic microstructure is shown in Fig. 1. Under symmetric loading condition, a one-eighth face-centred cuboidal cell can be chosen for FE analysis due to the periodic symmetry of the problem. The periodic symmetry requirements are satisfied by imposing the following constraint equations on the corresponding surfaces of the cell

$$u_x = 0 \quad t_y = t_z = 0 \quad \text{at } x = 0 \tag{1a}$$

$$u_y = 0 \quad t_x = t_z = 0 \quad \text{at } y = 0 \tag{1b}$$

$$u_z = 0 \quad t_x = t_y = 0 \quad \text{at } z = 0 \tag{1c}$$

$$u_x = U_{x0} \quad t_y = t_z = 0 \quad \text{at } x = a \tag{2a}$$

$$u_y = U_{y0} \quad t_x = t_z = 0 \quad \text{at } y = a \tag{2b}$$

$$u_z = U_{z0} \quad t_x = t_y = 0 \quad \text{at } z = a \tag{2c}$$

where a is the cell length, u_x, u_y and u_z are components of the displacement vector $\boldsymbol{u}$ along x-, y- and z-directions, t_x, t_y, and t_z are components of surface traction $\boldsymbol{t}$ along x-, y- and z-directions, U_{x0}, U_{y0}, and U_{z0} are displacement constants. The surfaces of $x = 0$, $y = 0$ and $z = 0$ are symmetric planes. The surfaces of $x = a$, $y = a$ and $z = a$ are maintained straight and move parallel with respect to their original shapes during deformation due to the periodic requirement.

TABLE I Material properties for matrix and rubber particles

Phase	Young's modulus (MPa)	Poisson's ratio	Yield stress (MPa)
Matrix	3500	0.25	80
Rubber particles	1–100	0.49–0.4999	–

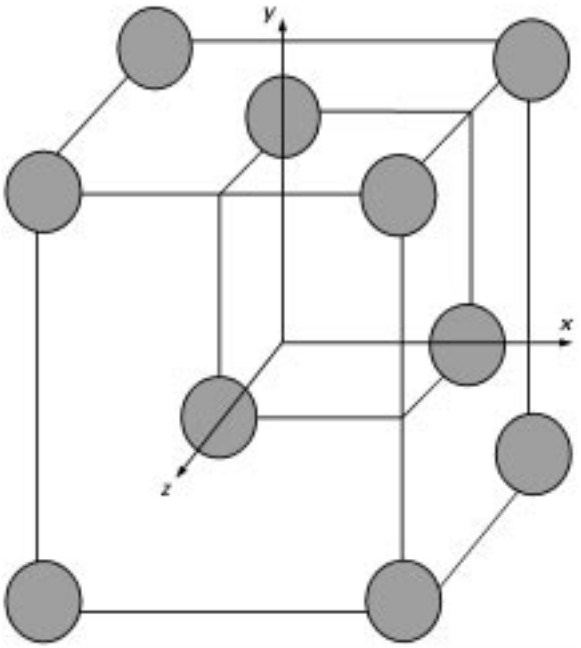

Figure 1 Three-dimensional periodic micromechanical model.

The effective stress, σ^e, and strain, ε^e, are obtained by averaging the local stress, σ, and strain, ε, in the cell, that is

$$\sigma^e = \frac{1}{V_\Omega}\int_{V_\Omega}\sigma\,dV = \frac{1}{V_\Omega}\int_{S_\Omega}\mathbf{r}\otimes\mathbf{t}\,dS \quad (3)$$

$$\varepsilon^e = \frac{1}{V_\Omega}\int_{V_\Omega}\varepsilon\,dV = \varepsilon^0 \quad (4)$$

where $\mathbf{r}$ is the position vector, $\mathbf{t}$ is the traction vector acting on the cell surface, ε^0 is the constant strain tensor dependent on the uniform normal displacement $\mathbf{U}_0$ on the cell surface, V_Ω and S_Ω represent the cell volume and surface, respectively. We use the equilibrium condition without volume forces, i.e. $\nabla\cdot\sigma = 0$, to obtain the last equality of Equation 3.

The effective elastic constants can be derived from the following expressions

$$\varepsilon^e_{xx} = \frac{1}{E^e}[\sigma^e_{xx} - \nu^e(\sigma^e_{yy} + \sigma^e_{zz})] \quad (5a)$$

$$\varepsilon^e_{yy} = \frac{1}{E^e}[\sigma^e_{yy} - \nu^e(\sigma^e_{zz} + \sigma^e_{xx})] \quad (5b)$$

$$\varepsilon^e_{zz} = \frac{1}{E^e}[\sigma^e_{zz} - \nu^e(\sigma^e_{xx} + \sigma^e_{yy})] \quad (5c)$$

where E^e is the effective Young's modulus and ν^e the effective Poisson's ratio. The effective bulk modulus can be calculated by the relation: $k^e = E^e/3(1-2\nu^e)$.

The effective stress triaxiality is defined by

$$R^e_\sigma \equiv \frac{\sigma^e_m}{\sigma^e_s} \quad (6)$$

where the effective mean stress $\sigma^e_m = \sigma^e{:}\,\mathbf{I}/3$, the effective Von Mises stress $\sigma^e_s = (3\mathbf{S}^e{:}\,\mathbf{S}^e/2)^{1/2}$, $\mathbf{S}^e$ is the deviatoric part of the effective stress σ^e, $\mathbf{S}^e = \sigma^e - \sigma^e_m\mathbf{I}$ [25].

We can obtain the local stress and strain fields at different effective stress triaxiality by adjusting the uniform normal displacement increments of each face of the cell to ensure that the average true stress on each face maintains the desired value [21]. In our calculations, U_{x0} is equal to U_{y0} and the transverse constraint parameter is defined by $\alpha = U_{x0}/U_{z0} = U_{y0}/U_{z0}$. The influence of effective stress triaxiality can be studied by varying the transverse constraint parameter. From Equations 5 and 6 we know that R^e_σ depends only on α and ν^e in the elastic regime. When α is kept constant, the surfaces $x = a$ and $y = a$ can move freely in the transverse direction. This corresponds to macroscopic uniaxial tension, that is, $\sigma^e_{zz} \neq 0$ and $\sigma^e_{xx} = \sigma^e_{yy} = 0$. $\alpha = 0$ corresponds to macroscopic uniaxial deformation (i.e. biaxial plane-strain condition) in which $\varepsilon^e_{zz} \neq 0$ and $\varepsilon^e_{xx} = \varepsilon^e_{yy} = 0$. $\alpha = 1$ corresponds to macroscopic equi-triaxial tension, that is, $\sigma^e_{xx} = \sigma^e_{yy} = \sigma^e_{zz}$.

3. Results and discussion

Four particle volume fractions of 0.209%, 1.676%, 13.40% and 26.18% were examined with respect to the particle radius to cell length ratio of 0.1, 0.2, 0.4 and 0.5. The PATRAN program was used to generate the mesh automatically in the one-eighth face-centred cuboidal cell for the four particle volume fractions. The undeformed mesh for the particle volume fraction of 26.18% is shown in Fig. 2. Three-dimensional large deformation elastoplastic finite element analysis was carried out for the particle/matrix system up to a macroscopic extension ratio of 35% incrementally by the ABAQUS program on an ALPHA STATION 500. For comparison, we also used the same mesh to do the calculations for the void/matrix system with rubber particles replaced by voids. True stress and logarithmic strain were used in the analysis.

3.1. Effects of particle volume fraction and effective stress triaxiality

By homogenization of the three-dimensional FE results, the effective stress–strain curves under macroscopic uniaxial tension at the particle volume fractions of 0.209%, 1.676%, 13.40% and 26.18% are plotted in Fig. 3. The dependence of effective Young's modulus, Poisson's ratio and yield stress normalized by the corresponding matrix mechanical property on the particle volume fraction obtained under macroscopic uniaxial tension is shown in Fig. 4. Particle Young's

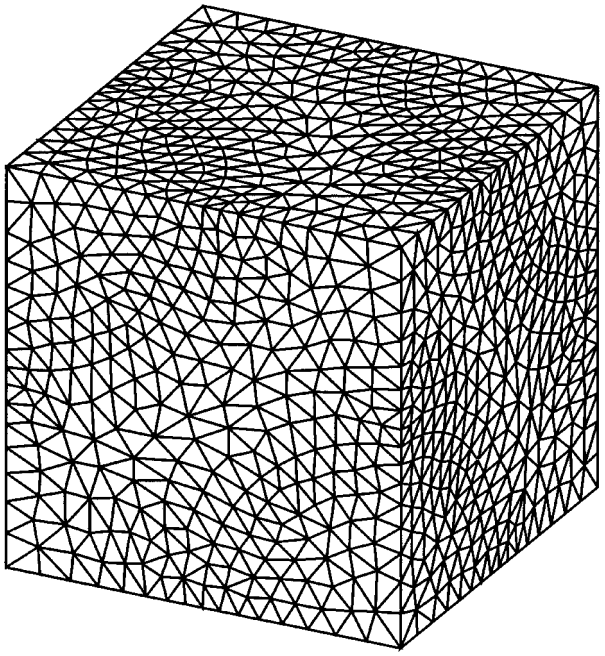

Figure 2 Undeformed mesh for the particle/matrix system with particle volume fraction $f_i = 26.18\%$.

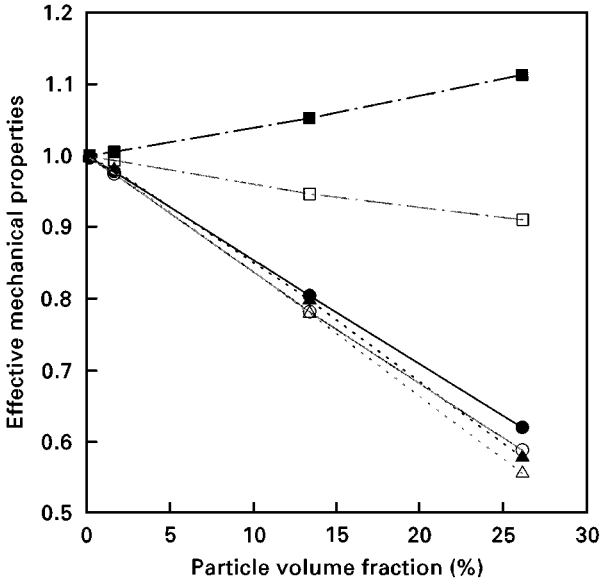

Figure 4 Normalized effective (●, ○) Young's modulus, (■, □) Poisson's ratio and (▲, △) yield stress versus particle volume fraction. (●, ■, ▲) rubber/matrix system; (○, □, △) void/matrix system.

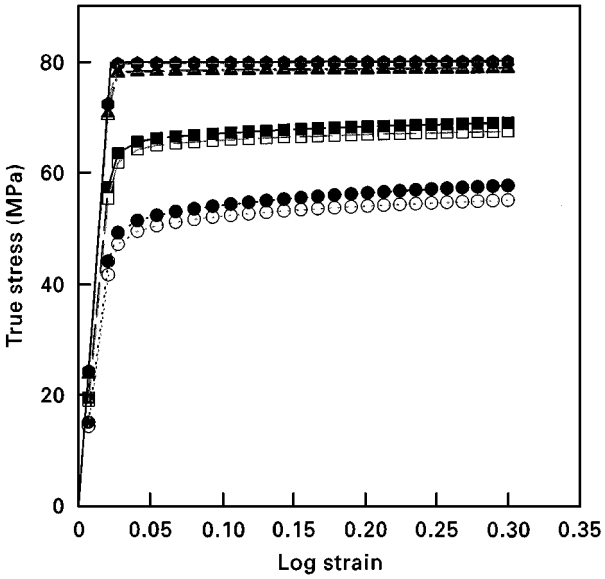

Figure 3 Effective stress–strain curves under macroscopic uniaxial tension at various particle volume fractions. (⬢, ▲, ■, ●) rubber/matrix system; (⬡, △, □, ○) void/matrix system. f_i: (——) 0, (⬡, ⬢) 0.21%, (▲, △) 1.68%, (■, □) 13.40%, (●, ○) 26.18%.

modulus is 2 MPa and Poisson's ratio is 0.499833 with a bulk modulus of 2000 MPa.

We can see that the level of effective stress decreases with increasing particle volume fraction. There is an apparent linear dependence of effective Young's modulus, Poisson's ratio and yield stress on particle volume fraction within the range we have examined. This trend is consistent with the uniaxial tensile Young's modulus and yield stress results obtained by Yee and Pearson [7]. Both the effective Young's modulus and yield stress decrease with increasing particle volume fraction. Effective Poisson's ratio increases with increasing particle volume fraction for the particle/matrix systems but decreases for the void/matrix systems. When compared with the two-dimensional plane-strain finite element results by Wu *et al.* [17], the effective stress obtained from the three-dimensional analysis reaches a higher magnitude. For example, the effective yield stress is about 20% higher for three-dimensional modelling than for two-dimensional plane-strain modelling at a particle volume fraction of 26%.

The predicted values for the effective Young's modulus at various particle volume fractions are compared with experimental data [7] and other theoretical results [1, 20, 26], as shown in Fig. 5. Here we use the same material properties as Yee and Pearson [7] and Kinloch and Guild [20]. Young's modulus of the epoxy matrix is 2965 MPa and Poisson's ratio is 0.375 with a bulk modulus of 3953 MPa. Young's modulus of rubber particles is 1 MPa and Poisson's ratio is 0.49992 with a bulk modulus of 2083 MPa. We can see that the face-centred cuboidal model results agree well with the experimental data (and much better than the spherical model). The small difference observed can be associated with the difference in the assumed and real distributions of the rubber particles for FEA and in experiment, respectively. It is further noted that both the fcc model results and experimental data lie between the approximate lower and upper limits calculated using the analysis of Ishai and Cohen [26] for a regular cubic packing; but the experimental data are much closer to the upper limit. The predicted values of effective Young's modulus by the spherical model [20] exceed Ishai and Cohen's approximate upper limit [26] and Voigt's upper bound obtained from the effective shear and bulk moduli using the rule of mixtures [1]. This discrepancy may arise from the removal of all directional interactions in the spherical model [20].

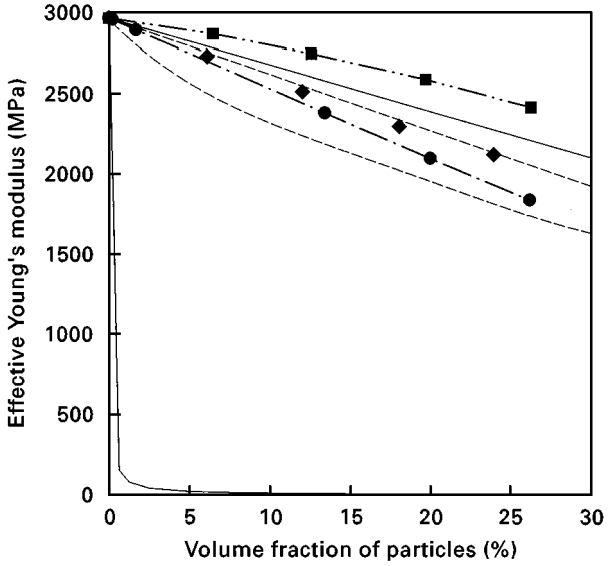

Figure 5 Comparison of (●) the predicted values for the effective Young's modulus at various particle volume fractions with (◆) experimental data [7] and other theoretical models. (——) rule of mixtures, Voigt and Reuss [1], (■) spherical modelling [20], (– – –) approximate limits [26].

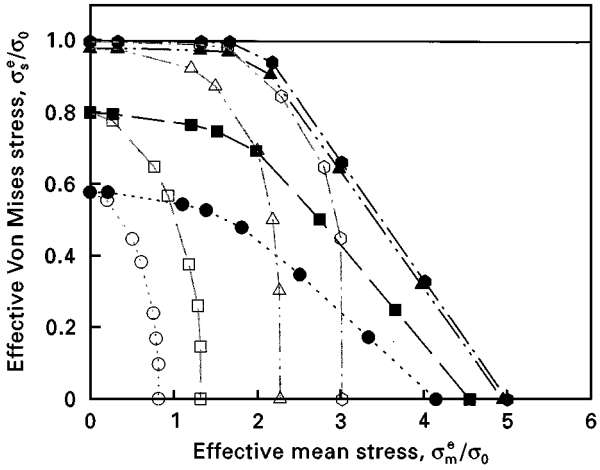

Figure 6 Profile of effective yield surface at various particle volume fractions. (⬢, ▲, ■, ●) rubber/matrix system; (⬡, △, □, ○) void/matrix system. f_i: (——) 0, (⬢, ⬡) 0.21%, (▲, △) 1.68%, (■, □) 13.40%, (●, ○) 26.18%.

However, it is more likely to be caused by the inappropriate way of calculating the effective Young's modulus from the ratio of the sum of all y-reactions-to-earth along AB and the y-strain as explained in Fig. 2 of [20]. According to Equations 3–5, under uniaxial tension, this ratio is equal to the effective Young's modulus for the square and cylindrical cell models. But this method of calculating the Young's modulus is not valid in general, and particularly for the spherical cell model. It is more appropriate to determine the effective Young's modulus and Poisson's ratio from Equation 5 using the definition of the effective stress and strain from Equations 3 and 4. We expect that the effective Young's modulus calculated from the spherical cell model using the appropriate Equations 3–5 will lie below the Voigt upper bound. But without performing the actual calculations, we cannot evaluate how close the predicted values will be to the experimental data.

The profiles of the effective initial yield surface for both particle/matrix and void/matrix systems are plotted in Fig. 6. Particle Young's modulus is 2 MPa and Poisson's ratio is 0.499833 with a bulk modulus of 2000 MPa. The shape of the effective initial yield surface for the particle/matrix system is different from that for the void/matrix system. This difference becomes larger with increasing particle volume fraction. At low triaxiality the effective initial yield stress for the particle/matrix and void/matrix systems is almost the same, while at high triaxiality it drops more rapidly for the latter than the former material system. These results confirm that particle cavitation is conducive to shear yielding at high triaxiality although it may not be important at low triaxiality.

The contour plots of hydrostatic pressure and Von Mises stress at a macroscopic extension ratio of 1.4% in the z-direction for the particle/matrix system with a particle volume fraction of 26.18% under macroscopic uniaxial tension (α is only a constant) and uniaxial deformation ($\alpha = 0$) are shown in Figs 7 and 8. The symbol " + " stands for compression and " − " for tension and all stresses are in MPa.

Rubber particles sustain almost constant dilatational stress whose magnitude is similar to the average dilatational stress while the Von Mises stress inside the rubber particles tends to zero. The matrix sustains compression near the pole and tension near the equator under macroscopic uniaxial tension; but it may also sustain tension under macroscopic uniaxial deformation. Maximum Von Mises stress in the matrix is reached at the equator of rubber particles with the shortest distance between particles. So shear yielding occurs there first. After that, the shear yielding zone shifts from the equator towards the 45° region around the particle–matrix interface and finally forms localized shear bands. These results are consistent with the observations in the PC/hole experiments by Sue and Yee [8]. Maximum dilatational stress in the matrix is also reached at the equator of rubber particles. With the application of transverse constraints the local dilatational stress increases while local Von Mises stress decreases. This shows that transverse constraint is beneficial for cavitation but it defers shear deformation.

The dependence of maximum dilatational stress, direct stress and Von Mises stress concentration factors on particle volume fraction under macroscopic uniaxial tension is shown in Fig. 9. The stress concentration factor is defined as the ratio of local stress to corresponding average stress in the elastic range. Clearly, all the three maximum stress concentration factors increase with increasing particle volume fraction. The void/matrix system has larger stress concentrations than the particle/matrix system. Maximum Von Mises stress and direct stress concentration factors are 1.91 and 2.08 under macroscopic uniaxial tension for the void/ matrix system with a particle volume fraction of 0.21%. Owing to the overlapping of stress fields between particles, the maximum

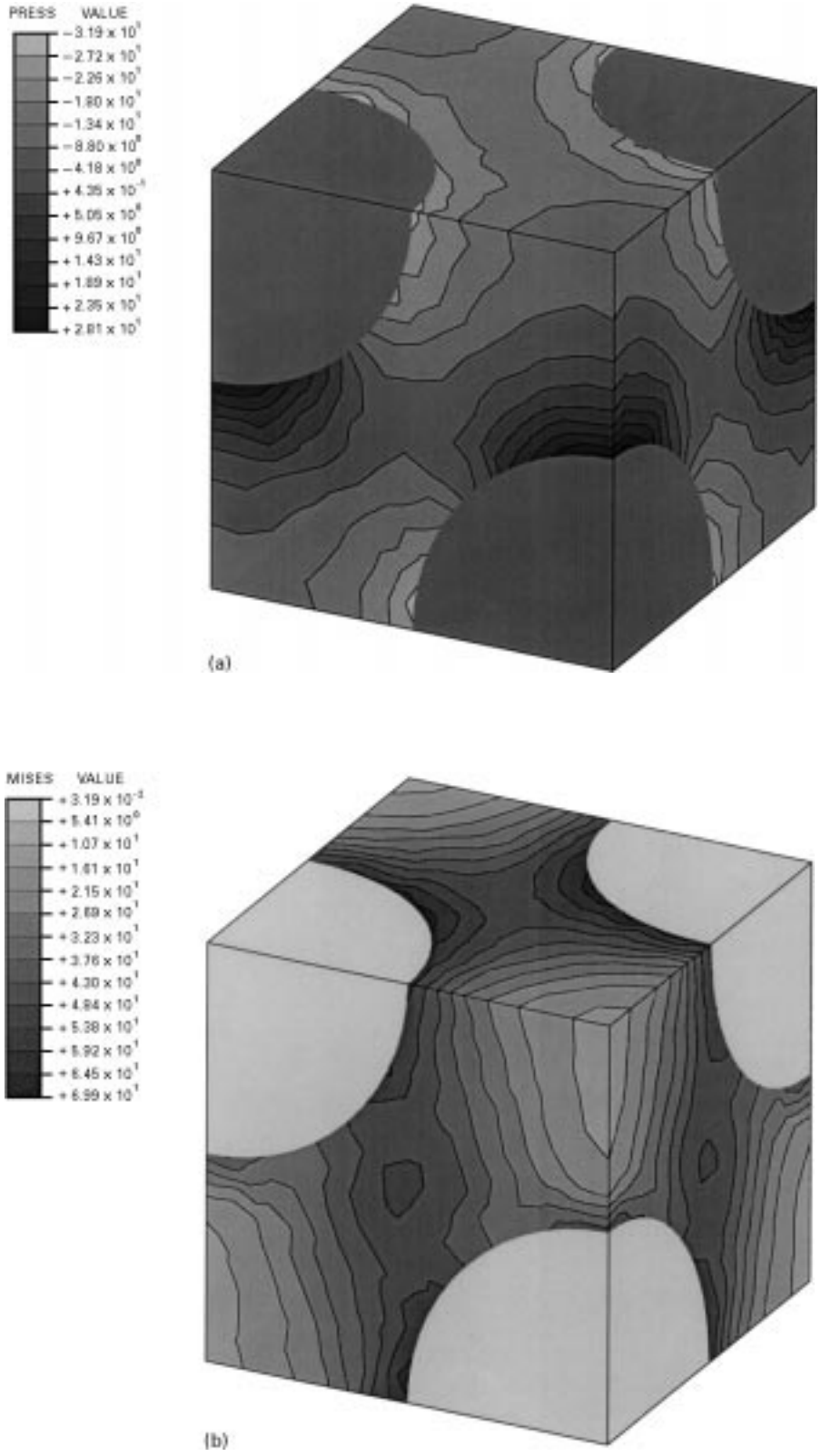

Figure 7 Contour plots of hydrostatic pressure and Von Mises stress for the particle/matrix system at a particle volume fraction of 26.18% under macroscopic *uniaxial tension* with a macroscopic extension ratio of 1.4% in the z-direction: (a) hydrostatic pressure, (b) Von Mises stress.

Von Mises stress and direct stress concentration factors increase to 2.47 and 2.67 at a particle volume fraction of 20%, respectively. Huang and Kinloch [13, 14] predicted the maximum Von Mises stress and direct stress concentrations to be 2.21 and 2.43 by the cylindrical model and 3.81 and 4.36 by the two-dimensional plane-strain model at a particle volume fraction of 19% (see Table II in [13, 14]). They showed a steady linear rise in the Von Mises stress concentration with particle volume fraction by two-dimensional plane-strain modelling but a slower increase up to a particle volume fraction of about 30% by cylindrical modelling. The fracture toughness of rubber-modified epoxy does indeed increase steadily with increasing rubbery volume fraction according to many experimental observations [13, 14]. In comparison, our three-dimensional

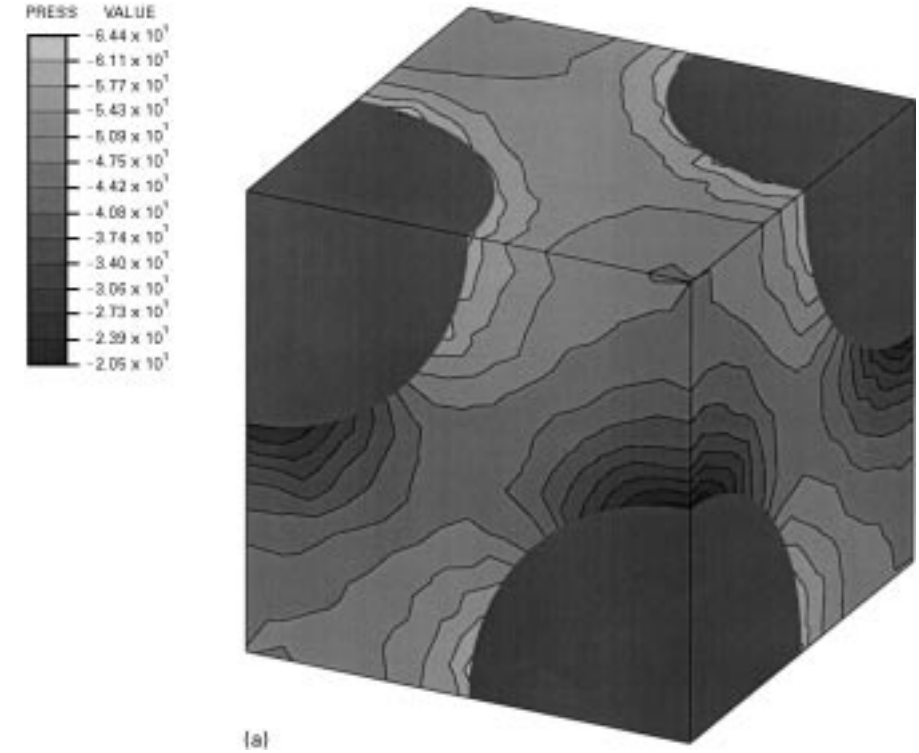

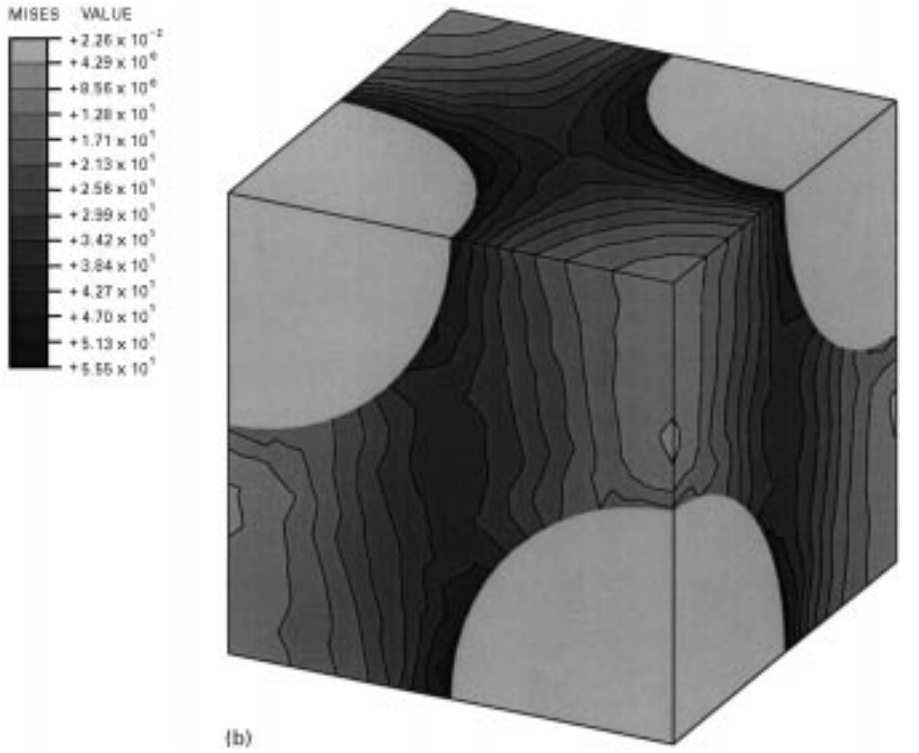

Figure 8 Contour plots of hydrostatic pressure and Von Mises stress for particle/matrix system at a particle volume fraction of 26.18% under macroscopic *uniaxial deformation* with a macroscopic extension ratio of 1.4% in the z-direction: (a) hydrostatic pressure, (b) Von Mises stress.

model shows that the axisymmetric model underestimates while the two-dimensional plane-strain model overestimates the increasing rate of stress concentrations with particle volume fraction.

The hydrostatic tension inside the rubber particles, maximum direct stress and maximum Von Mises stress in the matrix at various effective stress triaxiality by the face-centred cuboidal cell model using three-dimensional elastic finite element analysis for the particle/matrix and void/matrix systems are shown in Table II. For comparison, we use the same material properties and elastic analysis as given in Guild and Kinloch [19]. The volume fraction of rubber particles or voids is 20%. The matrix has Young's modulus of 3000 MPa, Poisson's ratio of 0.35 and bulk modulus of 3333 MPa. For the rubber particles, the Young's

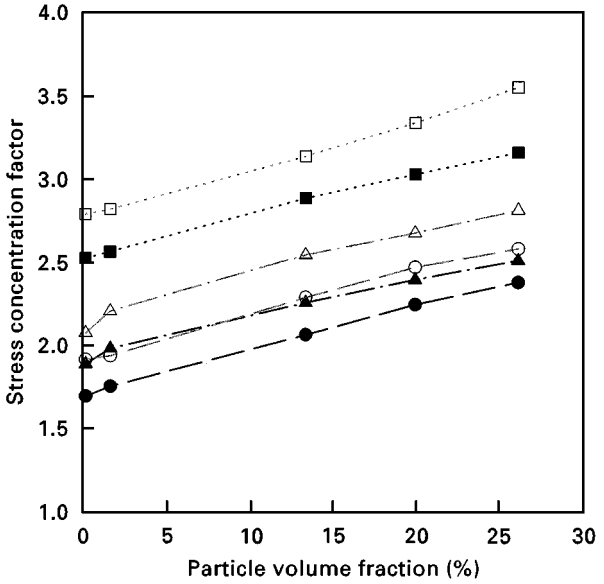

Figure 9 Maximum stress concentrations versus particle volume fraction under macroscopic uniaxial tension. (●, ■, ▲) rubber/matrix system, (○, □, △) void/matrix system. (●, ○) Von Mises, (■, □) mean stress, (▲, △) direct stress.

modulus is 1 MPa, Poisson's ratio 0.4999 and bulk modulus 2083 MPa. The calculated effective Young's moduli are 2119 and 2025 MPa and Poisson's ratios 0.3833 and 0.3231 for the particle/matrix and void/matrix systems, respectively. The effective stress was kept at 100 MPa in the z-direction and but varied in the x- and y-directions.

Hydrostatic tension inside the rubber particles increases, while maximum direct stress and Von Mises stress in the matrix decrease with increasing lateral tension in the x- and y-directions for the rubber particle/matrix system. From Table II we can see that the spherical model gives a good prediction of the hydrostatic tension inside rubber particles but somewhat lower increasing rate of the direct stress and Von Mises stress concentrations in the matrix as the effective stress triaxiality decreases compared with the three-dimensional model. For example, the three-dimensional model predicts the maximum direct and Von Mises stresses in the matrix increase by a factor of 1.43 and 3.93 as the effective stress system varies from 100 : 100 : 100 MPa to 60 : 60 : 100 MPa, while the values predicted by the spherical model are only 1.27 and 3.02. Maximum direct stress and Von Mises stress are much higher for the void/matrix system than for the rubber particle/matrix system under a given effective stress system. The difference in the local stress fields between the rubber particle/matrix and void/matrix systems becomes larger with increasing effective stress triaxiality.

It has been demonstrated that a high tensile triaxial stress state is helpful for rubber cavitation. However, it defers the development of matrix shear deformation in the particle/matrix system. After cavitation, the local Von Mises stress in the matrix increases substantially at high triaxiality. Owing to the high triaxiality near a crack tip, rubber particles in the neighbourhood can sustain much higher hydrostatic tension than particles located elsewhere and so they can easily cavitate before shear yielding occurs in the surrounding matrix. Therefore, rubber cavitation is essential to promote extensive plastic deformation in a toughening process at high triaxiality, although it may not be important at low triaxiality.

3.2. Effects of particle Young's modulus

The dependence of the effective Young's modulus, Poisson's ratio, bulk modulus and yield stress normalized by the corresponding matrix mechanical property on the particle Young's modulus at a particle volume fraction of 26.18% obtained under macroscopic uniaxial tension is shown in Fig. 10. The particle Poisson's ratio is 0.499833. All the effective Young's modulus, Poisson's ratio, bulk modulus and yield stress increase with increasing particle Young's

TABLE II Effects of effective stress triaxiality on hydrostatic tension inside rubber particles and maximum direct stress and Von Mises stress in the matrix

σ^e_{xx}: σ^e_{yy}: σ^e_{zz} (MPa)	R^e_σ	Hydrostatic tension inside rubber particles (MPa)		Maximum direct stress in matrix (MPa)		Maximum Von Mises stress in matrix (MPa)	
		3-D	[19]	3-D	[19]	3-D	[19]
Particles							
100 : 100 : 100	$+\infty$	85.6	87.1	112.9	111.3	24.3	24.1
90 : 90 : 100	9.333	80.5	81.3	125.2	118.8	35.5	32.4
80 : 80 : 100	4.333	75.1	75.5	137.2	126.2	53.6	44.6
70 : 70 : 100	2.667	69.6	69.7	149.1	133.7	73.4	58.4
60 : 60 : 100	1.833	63.8	63.9	161.9	141.2	95.6	72.7
0 : 0 : 100	0.333	29.0		232.9		222.9	
Voids							
100 : 100 : 100	$+\infty$	–	–	208.3	187.7	187.1	187.4
90 : 90 : 100	9.333	–	–	215.1	190.0	179.8	181.9
80 : 80 : 100	4.333	–	–	219.8	192.4	177.6	177.7
70 : 70 : 100	2.667	–	–	225.5	194.8	178.0	174.8
60 : 60 : 100	1.833	–	–	231.2	197.2	181.6	173.3
0 : 0 : 100	0.333			265.2		246.5	

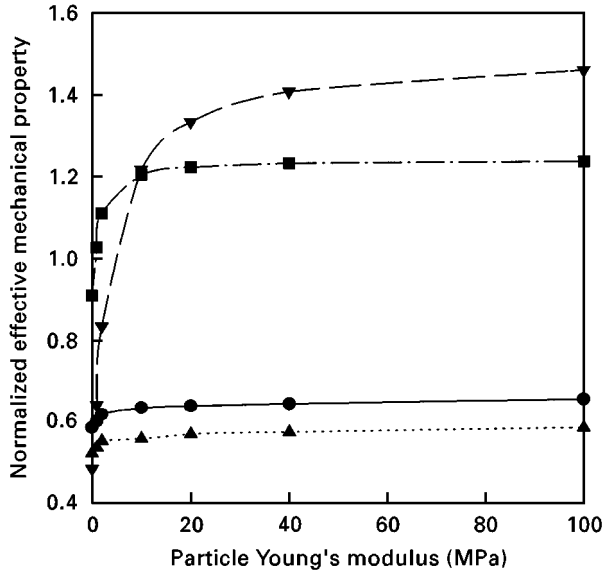

Figure 10 Normalized effective mechanical properties versus particle Young's modulus. (●) E^c/E_m, (■) ν^c/ν_m, (▼) k^c/k_m, (▲) σ_s^c/σ_m.

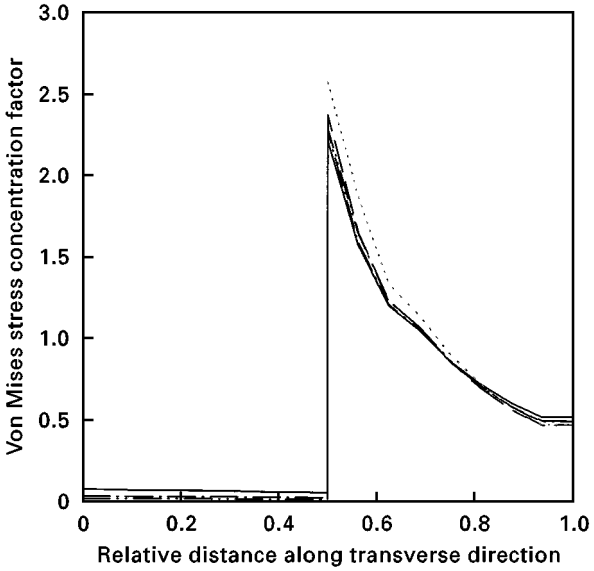

Figure 12 Von Mises stress concentration factor versus relative distance along the transverse direction under macroscopic uniaxial tension for various particle Young's moduli. For key, see Fig. 11.

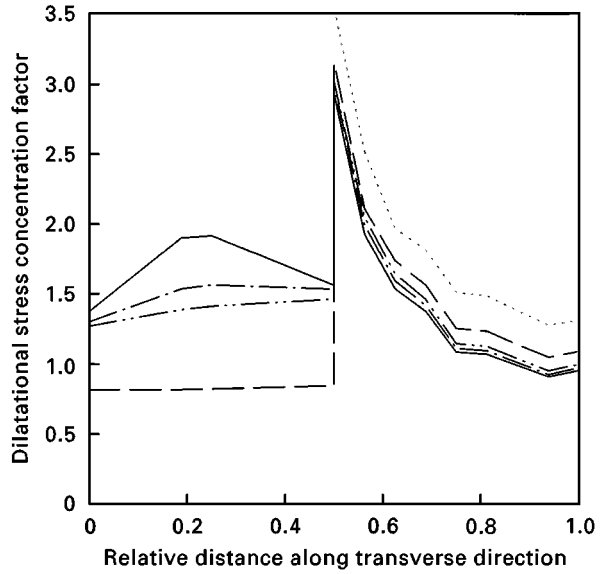

Figure 11 Dilatational stress concentration factor versus relative distance along the transverse direction under macroscopic uniaxial tension for various particle Young's moduli, E_i: (——) 100 MPa, (— - —) 40 MPa, (— - - —) 20 MPa, (— —) 2 MPa, (···) voids.

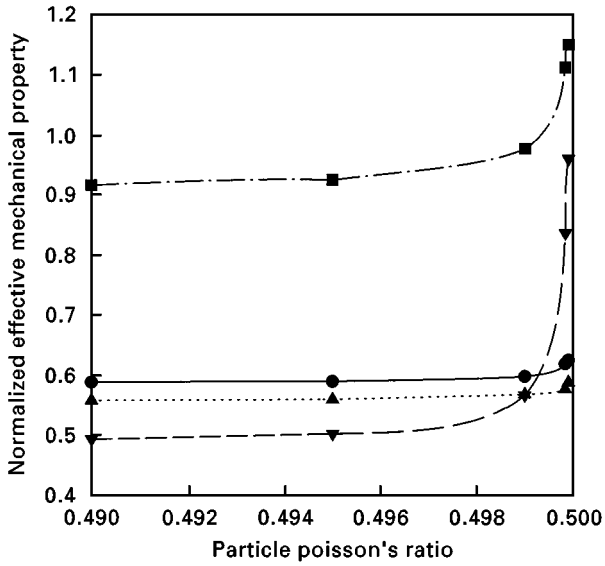

Figure 13 Normalized effective mechanical properties versus particle Poisson's ratio. (●) E^c/E_m, (■) ν^c/ν_m, (▼) k^c/k_m, (▲) σ_s^c/σ_m.

modulus. As the particle Young's modulus exceeds 2 MPa, the effective Young's modulus and yield stress approach their asymptotic values, respectively.

The distribution of dilatational and Von Mises stress concentration factors along the path from the centre of one rubber particle to the nearest corner of the cell in the transverse direction under macroscopic uniaxial tension at various particle Young's moduli, are shown in Figs 11 and 12, respectively. Both dilatational and Von Mises stress concentration factors decrease with increasing particle Young's modulus in the matrix but increase inside the particles. The particle Young's modulus has a distinguishable influence on the dilatational stress concentration factor inside the particles. As the particle Young's modulus increases from 2 MPa to 20 MPa, the dilatational stress concentration factor at the centre of particles increases from 0.82 to 1.27.

3.3. Effects of particle Poisson's ratio

The dependence of the effective Young's modulus, Poisson's ratio, bulk modulus and yield stress normalized by the corresponding matrix mechanical property on the particle Poisson's ratio at a particle volume fraction of 26.18% obtained under macroscopic uniaxial tension, is shown in Fig. 13. The particle Young's modulus is 2 MPa. There is only a small increase of the effective Young's modulus and yield stress as the particle Poisson's ratio increases from 0.49 to 0.4999, while the effective bulk modulus and Poisson's ratio increase rapidly as the particle

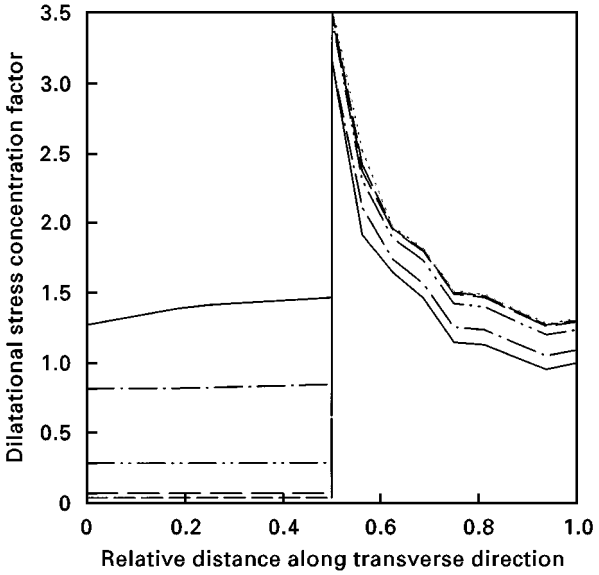

Figure 14 Dilatational stress concentration factor versus relative distance along the transverse direction under macroscopic uniaxial tension for various particle Poisson's ratios, ν_i: (——) 0.4999, (— - —) 0.499833, (— - - —) 0.499, (— —) 0.495, (– –) 0.49, (· · ·) voids.

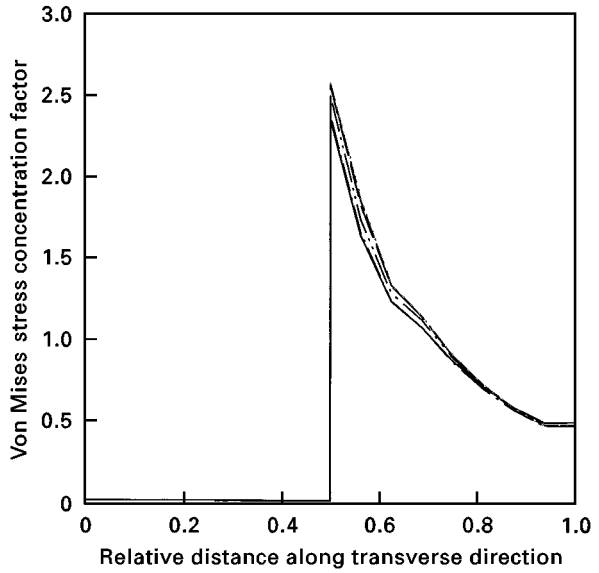

Figure 15 Von Mises stress concentration factor versus relative distance along the transverse direction under macroscopic uniaxial tension for various particle Poisson's ratios. For key, see Fig. 14.

Poisson's ratio exceeds 0.499. The effective bulk modulus doubles as the particle Poisson's ratio increases from 0.49 to 0.4999.

The distribution of the dilatational and Von Mises stress concentration factors along the path from the centre of one rubber particle to the nearest corner of the cell in the transverse direction under macroscopic uniaxial tension at various particle Poisson's ratio is shown in Figs 14 and 15, respectively. The effect of particle Poisson's ratio on the local stress concentration factors is similar to that of particle Young's modulus. Both dilatational and Von Mises stress concentration factors decrease with increasing particle Poisson's ratio in the matrix while they increase inside the rubber particles. Particle Poisson's ratio has a notable influence on the dilatational stress concentration factor inside rubber particles. As the particle Poisson's ratio increases from 0.49 to 0.4998, the dilatational stress concentration factor inside rubber particles increases from 0.035 to 0.82.

4. Conclusions

We have studied the effects of phase morphology and mechanical properties of rubber particles on the local stress and strain fields and the effective stress–strain relations using our new micromechanical model. The following conclusions can be drawn.

1. The level of effective stress decreases with increasing particle volume fraction under macroscopic uniaxial tension. The effective Young's modulus and yield stress decrease with increasing particle volume fraction. The effective Poisson's ratio increases with increasing particle volume fraction for the particle/matrix system but decreases for the void/matrix system. It is shown that the two-dimensional plane-strain model underestimates the effective stress compared with the three-dimensional model at the same particle volume fraction.

2. The effective yield stress depends greatly on stress triaxiality. The shapes of the effective initial yield surface for the particle/matrix and void/matrix systems are different from each other. This difference becomes larger with increasing particle volume fraction. At low stress triaxiality, the effective yield stresses for both particle/matrix and void/matrix systems are almost the same; but at high stress triaxiality, the effective yield stress drops more rapidly in the latter than the former system. These results confirm that rubber cavitation is beneficial to matrix shear yielding at high triaxiality although it may not be important at low triaxiality.

3. All the maximum dilatational stress, direct stress and Von Mises stress concentration factors in the matrix increase steadily with increasing particle volume fraction under macroscopic uniaxial tension. Inside the rubber particles, the Von Mises stress tends to zero while the dilatational stress is almost constant with the same order of magnitude as that of the matrix because rubber has a low shear modulus and a high bulk modulus. When compared with the three-dimensional model results, the axisymmetric model underestimates while the two-dimensional plane-strain model overestimates the increasing rate of the maximum stress concentrations in the matrix with particle volume fraction.

4. High triaxial stress state promotes rubber cavitation but discourages the development of shear deformation in the matrix for the particle/matrix system. Relative to the three-dimensional model, the spherical model gives good predictions of the hydrostatic tension inside the rubber particles but yields somewhat lower maximum stress concentrations in the matrix at low effective stress triaxiality. The maximum direct stress and Von Mises stress for the void/matrix system are higher than those for the particle/matrix system under a set of applied stresses. The difference in the

local stress fields between the particle/matrix and void/matrix systems becomes significant with increasing stress triaxiality. Rubber particles near a crack tip are easy to cavitate due to the high stress triaxiality there, so that extensive plastic deformation can be developed in the matrix.

5. All the effective Young's modulus, Poisson's ratio, bulk modulus and yield stress increase with increasing particle Young's modulus and Poisson's ratio. Both dilatational and Von Mises stress concentration factors decrease with increasing particle Young's modulus and Poisson's ratio in the matrix but increase inside the rubber particles. The higher the particle bulk modulus, the larger is the dilatational stress inside the rubber particles and so the easier they cavitate.

Acknowledgements

The authors thank the Australian Research Council (ARC) for the continuing support of the polymer blends project. Xiao-hong Chen is supported by a Postdoctoral Research Fellowship funded by the ARC.

References

1. J. ABOUDI, "Mechanics of Composite Materials: A Unified Micromechanical Approach", (Elsevier Science, Amsterdam, 1991) Chs 1–3.
2. P. TONG and C. C. MEI, *Comput. Mech.* **9** (1992) 195.
3. C. B. BUCKNALL, "Toughened Plastics", (Applied Science, London, 1977).
4. A. C. GARG and Y.-W. MAI, *Compos. Sci. Technol.* **31** (1988) 179.
5. C. K. RIEW and A. J. KINLOCH, "Toughened Plastics I", Advances in Chemistry Series 233 (American Chemical Society, Washington, DC, 1993).
6. A. J. KINLOCH, S. J. SHAW and D. A. TOD, *Polymer* **24** (1983) 1341.
7. A. F. YEE and R. A. PEARSON, *J. Mater. Sci.* **21** (1986) 2462.
8. H. J. SUE and A. F. YEE, *Polymer* **29** (1988) 1619.
9. D. S. PARKER, H. J. SUE, J. HUANG and A. F. YEE, *ibid.* **31** (1990) 2267.
10. A. F. YEE, D. LI and X. LI, *J. Mater. Sci.* **28** (1993) 6392.
11. J. S. WU and Y.-W. MAI, *ibid.* **28** (1993) 6167.
12. F. J. GUILD and R. J. YOUNG, *ibid.* **24** (1989) 2454.
13. Y. HUANG and A. J. KINLOCH, *ibid.* **27** (1992) 2753.
14. *Idem.*, *ibid.* **27** (1992) 2763.
15. *Idem.*, *Polymer* **33** (1992) 5338.
16. C. B. BUCKNALL, A. KARPODINIS and X. C. ZHANG, *J. Mater. Sci.* **29** (1994) 3377.
17. Y. S. WU, J. S. WU and Y.-W. MAI, in "Fatigue and Fracture Mechanics", Vol. 28, ASTM STP 1321, edited by J. H. Underwood, B. D. MacDonald and M. R. Mitchell (American Society for Testing and Materials, Philadelphia, PA, 1997) p. 671.
18. *Idem.*, in "Proceedings of the Materials Research 96", Vol. 1, IMMA, 10–12 July 1996, Queensland, p. 153.
19. F. J. GUILD and A. J. KINLOCH, *J. Mater. Sci.* **30** (1995) 1689.
20. A. J. KINLOCH and F. J. GUILD, in "Toughened Plastics II", edited by C. K. Riew and A. J. Kinloch, Advances in Chemistry Series 252 (American Chemical Society, Washington, DC, 1996) p. 1.
21. C. L. HOM and R. M. McMEEKING, *J. Appl. Mech.* **56** (1989) 309.
22. H.-J. SUE and A. F. YEE, *Polym. Eng. Sci.* **36** (1996) 2320.
23. X.-H. CHEN and P. TONG, unpublished research report (1995), Department of Mechanical Engineering, Hong Kong University of Science and Technology, Hong Kong.
24. X.-H. CHEN and Y.-W. MAI, *Key Eng. Mater.* **137** (1998) 115.
25. "ABAQUS/Standard User's Manual", Version 5.5 (Hibbitt, Karlsson and Sorensen, RI, USA, 1995) Vol. I, Ch 4.
26. O. ISHAI and L. J. COHEN, *Int. J. Mech. Sci.* **9** (1967) 539.

Received 12 September 1997
and accepted 22 April 1998